Liu *et al. Biology Direct* (2024) 19:78
https://doi.org/10.1186/s13062-024-00519-5

Biology Direct

RESEARCH

Open Access

Equol exerts anti-tumor effects on choriocarcinoma cells by promoting TRIM21-mediated ubiquitination of ANXA2

Xiao-Mei Liu[1], Zi-Hao Wang[1], Qian-Xue Wei[1], Yang Song[1] and Xiao-Xin Ma[1*]

Abstract

Choriocarcinoma is a malignant cancer that belongs to gestational trophoblastic neoplasia (GTN). Herein, serum metabolomic analysis was performed on 29 GTN patients and 30 healthy individuals to characterize the metabolic variations during GTN progression. Ultimately 24 differential metabolites (DMs) were identified, of which, Equol was down-regulated in GTN patients, whose VIP score is the 3rd highest among the 24 DMs. As an intestinal metabolite of daidzein, the anticancer potential of Equol has been demonstrated in multiple cancers, but not choriocarcinoma. Hence, human choriocarcinoma cell lines JEG-3 and Bewo were used and JEG-3-derived subcutaneous xenograft models were developed to assess the effect of Equol on choriocarcinoma. The results suggested that Equol treatment effectively suppressed choriocarcinoma cell proliferation, induced cell apoptosis, and reduced tumorigenesis. Label-free quantitative proteomics showed that 136 proteins were significantly affected by Equol and 20 proteins were enriched in Gene Ontology terms linked to protein degradation. Tripartite motif containing 21 (TRIM21), a E3 ubiquitin ligase, was up-regulated by Equol. Equol-induced effects on choriocarcinoma cells could be reversed by TRIM21 inhibition. Annexin A2 (ANXA2) interacted with TRIM21 and its ubiquitination was modulated by TRIM21. We found that TRIM21 was responsible for proteasome-mediated degradation of ANXA2 induced by Equol, and the inhibitory effects of Equol on the malignant behaviors of choriocarcinoma cells were realized by TRIM21-mediated down-regulation of ANXA2. Moreover, β-catenin activation was inhibited by Equol, which also depended on TRIM21-mediated down-regulation of ANXA2. Taken together, Equol may be a novel candidate for the treatment for choriocarcinoma.

Keywords ANAX2, Choriocarcinoma, Equol, Metabolomics, Proteomics, TRIM21

*Correspondence:
Xiao-Xin Ma
maxx@sj-hospital.org
Full list of author information is available at the end of the article

Graphical abstract

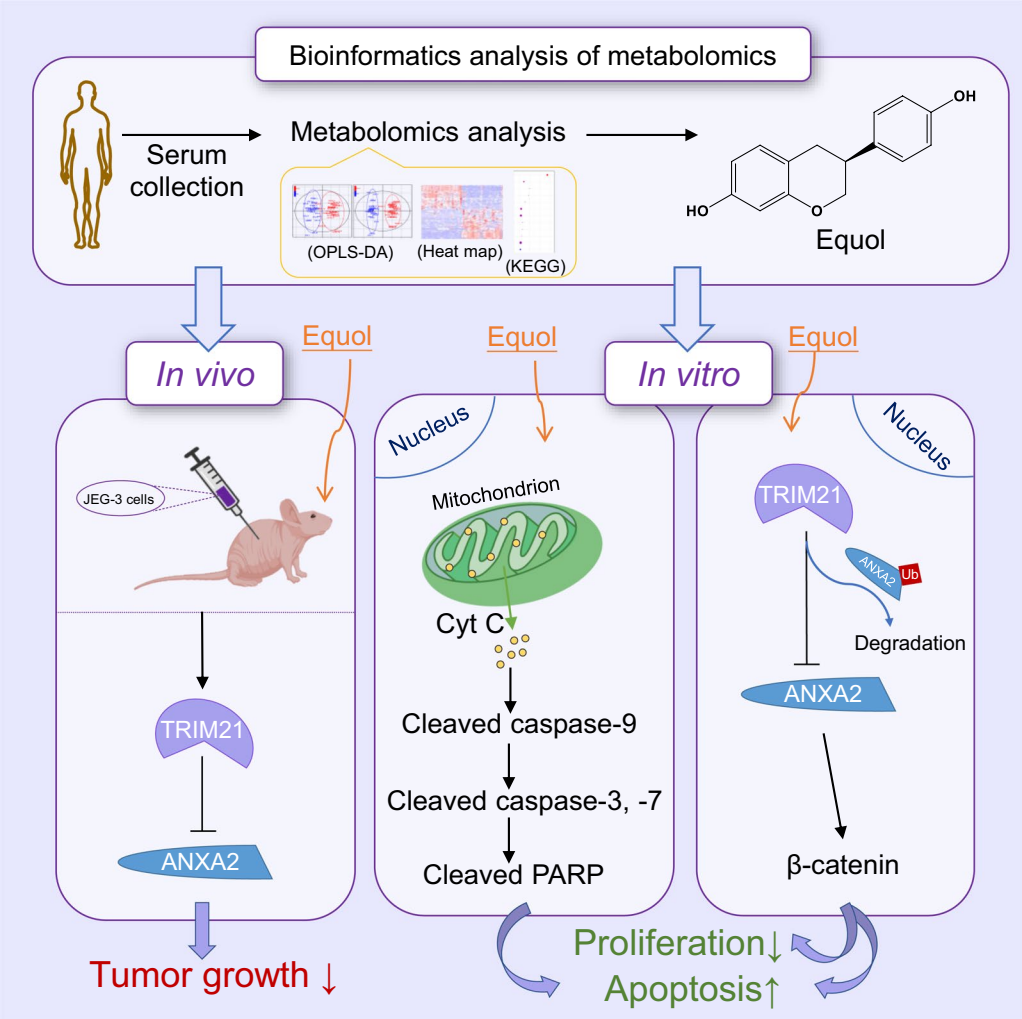

Introduction

Gestational trophoblastic neoplasia (GTN) refers to four malignant forms of gestational trophoblastic disease, comprising invasive mole, choriocarcinoma, placental site trophoblastic tumor and epithelioid trophoblastic tumor [1, 2]. All four related tumors arise from trophoblastic cells and develop in the placenta, of which invasive mole and choriocarcinoma are the most common cases [2]. Clinically, patients with choriocarcinoma are usually sensitive to chemotherapy, with the cure rate over 90% [3]. However, a few patients develop drug-resistance or relapse, and eventually succumb to multiple organ metastasis [2]. Thus, developing a new pathogenesis and optimizing the therapeutics for choriocarcinoma are greatly important for improving the prognosis of patients with GTN.

Equol is a nonsteroidal estrogen metabolized from soy isoflavone daidzein by microflora in the intestines [4]. In 1984, the possible roles of Equol in hormone-dependent diseases were first proposed by Dr. KDR Setchell and collaborators [5]. Afterwards, the anti-cancer property of Equol on androgen- or estrogen-mediated carcinomas has been widely discussed [6–8]. For example, Equol potently suppressed cell proliferation and induced apoptosis in androgen-dependent human prostate cancer LNCaP cells [6]. These encouraging biological activities of Equol have been reported for breast cancer [7]. Furthermore, previous study also revealed that Equol could inhibit proliferation of mouse melanoma B16 cells in an estrogen-independent manner [9]. In addition, Equol has been shown to induce mitochondria-mediated apoptosis

of cervical cancer and gastric cancer cells [10, 11]. However, its anti-tumor effect and precise mechanisms in choriocarcinoma have not been clarified.

The tripartite motif (TRIM) protein family is composed of 80 proteins with a highly conserved order of domains including a RING domain, one or two B-box domains, and a coiled-coil domain [12]. The presence of the RING domain endows with the ability to TRIM proteins, which mediates the attachment of ubiquitin or small ubiquitin-like modifier (SUMO) to target proteins [13, 14]. TRIM21 (also known as RO52), a member of the TRIM protein family, was first identified as an autoantigen linked to autoimmune diseases [15]. The anti-cancer activity of TRIM21 has been reported in multiple types of cancer, including hepatocellular carcinoma [16], renal carcinoma [17], and breast cancer [18]. Nevertheless, the function of TRIM21 in choriocarcinoma remains to be elucidated.

In this study, serum metabolomic analysis was performed to discover GTN-related differential metabolites (DMs). Equol was identified as a down-regulated DM in GTN patients. Next, we further performed both in vivo and in vitro experiments to discover the potential effect of Equol on human choriocarcinoma cells and its underlying mechanisms.

Materials and methods

Reagents and antibodies

Equol (CAS: 94105-90-5) was purchased from Aladdin Reagent (Shanghai, China). The Caspase-3 Activity Assay Kit (C1116), the Cell Cycle Analysis Kit (C1052) and the Mitochondrial Membrane Potential Assay Kit (JC-1, C2006) were obtained from Beyotime Biotechnology (Shanghai, China). The Annexin V-FITC/PI Apoptosis Kit (KGA106) and the cell counting kit-8 (CCK-8; KGA317) were purchased from KeyGen Biotech Co., Ltd. (Nanjing, China). The Diaminobenzidine Kit (DAB-1031) was purchased from Maixin Inc. (Fujian, China). The MagicOmics Micro Proteomics Sample Preparation Kit (MagicOmics-MMB) was purchased from QLBIO (Beijing, China). Antibodies against ubiquitin (A19686) were acquired from ABclonal Technology (Wuhan, China). Anti-cleaved caspase-3 (AF7022) antibodies were purchased from Affinity Biosciences (Changzhou, China). Antibodies against cleaved caspase-7 (#8438), cleaved caspase-9 (#20750), and cleaved poly (ADP-ribose) polymerase (cleaved PARP, #5625) were obtained from CST Company (Danvers, MA, USA). Anti-cytochrome C (Cyt C, 10993-1-AP), Anti-TRIM21 (12108-1-AP), and Anti-GAPDH (60004-1-Ig) antibodies were acquired from Proteintech Group, Inc. (Wuhan, China). HRP-conjugated Goat Anti-Rabbit IgG (SE134) and Goat Anti-Mouse IgG (SE131) antibodies used for western blotting were purchased from Solarbio (Beijing, China). HRP-conjugated Goat Anti-Rabbit IgG (#31460) and Goat Anti-Mouse IgG (#31430) antibodies used for immunohistochemistry were purchased from Solarbio (Pittsburgh, PA, USA). CY3-conjugated Goat Anti-Rabbit IgG (ab6939) and FITC-conjugated Goat Anti-Mouse IgG (ab6785) antibodies were purchased from Abcam (Cambridge, UK). In addition, Anti-Annexin A2 (ANXA2, sc-28385) antibodies were obtained from Santa Cruz Biotechnology (CA, USA).

Clinical sample collection and untargeted metabolomic analysis

Serum samples were collected from 29 GTN (20 invasive mole and 9 choriocarcinoma) patients and 30 normal healthy individuals attending the Shengjing Hospital of China Medical University after the written informed consent to participate was obtained. All experiments were conducted with the approval of the Ethics Committee of Shengjing Hospital of China Medical University for Ethical Review.

We conducted the untargeted metabolomics using ultra-high performance liquid chromatography coupled with high-resolution mass spectrometry. Fifty milligrams of samples were weighted to an EP tube. After the addition of 1000 μL of extract solvent (acetonitrile:methanol:water, 2:2:1, containing 1 μg/mL of internal standard 2-Chloro-L-phenylalanine), the samples were vortexed for 30 s, homogenized at 45 Hz for 4 min, and sonicated for 5 min in ice-water bath. The homogenate and sonicate circle were repeated for 3 times, followed by incubation at −20 °C for 1 h and centrifugation at 12,000 rpm and 4 °C for 15 min. The resulting supernatants were transferred to LC–MS vials and stored at −80 °C for UHPLC-QE Orbitrap/MS analysis. LC–MS/MS analyses were performed using an UHPLC system (1290, Agilent Technologies) with a UPLC HSS T3 column (2.1 mm × 100 mm, 1.8 μm) coupled to Q Exactive (Orbitrap MS, ThermoFisher Scientific, Pittsburgh, PA, USA). The injection volume was 2 μL. The mobile phase A was 0.1% formic acid in water for positive, and 5 mmol/L ammonium acetate in water for negative, and the mobile phase B was acetonitrile. The preprocessing results generated a data matrix that consisted of the retention time (RT), mass-to-charge ratio (m/z) values, and peak intensity. OSI-SMMS (version 1.0, Dalian Chem Data Solution Information Technology Co. Ltd.) was used for peak annotation after XCMS data processing with in-house MS/MS database. Based on the orthogonal projection to latent structures-discriminant analysis (OPLS-DA) models, the variable importance in projection (VIP) scores were obtained. The metabolites with Log_2fold changes (Log_2FC) > 1.5, P-value < 0.05, and VIP ≥ 1 were considered to be differential metabolites (DMs). The Kyoto Encyclopedia of Genes and Genomes

(KEGG) enrichment analysis was conducted to uncover the biological pathways associated with DMs.

Choriocarcinoma cell lines and cell transfection

Human choriocarcinoma cell lines JEG-3 and Bewo were purchased from Procell Life Science & Technology Co., Ltd. (Wuhan, China), which were cultured in MEM (Solarbio) and Ham's F-12 K (Servicebio Biotechnology, Wuhan, China) mediums supplemented with 10% fetal bovine serum, respectively. Cells were maintained in a 37 °C cell incubator with an atmosphere of 5% CO_2. Both JEG-3 and Bewo cells were transfected with the small interference RNA (siRNA) targeting TRIM21 (siTRIM21) or co-transfected with siTRIM21 and the siRNA targeting ANXA2 (siANXA2) using Lipofectamine 3000 (Invitrogen, CA, USA), according to the manufacturer's instructions.

Cell viability assay

Cells were treated with desired concentrations of Equol (0–512 μM) for 24 h, transfected with siTRIM21, or co-transfected with siTRIM21 and siANXA2 for 48 h. The transfected cells were then treated with 40 μM Equol for 24 h. Cell viability was detected by CCK-8 assay, according to the manufacturer's protocol. The optical density at 450 nm was recorded by an 800™ TS microplate reader (BioTek, CA, USA).

Cell cycle assay

JEG-3 and Bewo cells were seeded into 6-well plates at a density of 4×10^5 cells per well and then treated with vehicle or Equol (20 μM and 40 μM) for 24 h. At the end of incubation, cells were harvested and fixed with 70% pre-cooled ethanol for 12 h, centrifuged, and then stained with propidium iodide utilizing a Cell Cycle Analysis Kit according to the manufacturer's introductions. Cell cycle was analyzed by a NovoCyte flow cytometer (ACEA Biosciences, San Diego, CA, USA).

Annexin V-FITC/PI apoptosis assay

JEG-3 and Bewo cells were seeded into 6-well plates (4×10^5 cells per well) and then treated under different conditions. Cells were directly treated with vehicle or Equol (20 μM and 40 μM) for 24 h, transfected with siTRIM21, or co-transfected with siTRIM21 and siANXA2 for 48 h. Then the transfected cells were treated with 40 μM Equol for 24 h. Subsequently, cells were harvested and stained with Annexin-V-FITC and PI, as described by the protocol for the Annexin V-FITC/PI Apoptosis Kit. Cell apoptosis was analyzed by utilizing a NovoCyte flow cytometer (ACEA Biosciences). For analysis, the annexin V-FITC$^+$/PI$^-$ cells were identified as early apoptotic cells, the annexin V-FITC$^+$/PI$^+$ cells as late apoptotic cells, and the annexin V-FITC$^-$/PI$^-$ cells as viable cells.

Western blot analysis

Cellular lysates were prepared using RIPA lysis buffer (Solarbio) containing Phenylmethylsulfonyl fluoride (PMSF, Solarbio). Proteins were resolved using sodium dodecyl sulfate polyacrylamide gel electrophoresis (SDS-PAGE) and transferred to Immobilon®-P PVDF membranes (Millipore, USA). The membranes were blocked with 5% (M/V) skim-milk in TBST buffer for 1 h at room temperature and then incubated with antibodies against cleaved caspase-3, cleaved caspase-7, cleaved caspase-9, cleaved PARP, Cyt C, TRIM21, ANXA2, and GAPDH at 4℃ overnight. After four washes, the membranes were incubated with the HRP-conjugated Goat Anti-Rabbit IgG and Goat Anti-Mouse IgG antibodies for 1 h at 37 °C. The proteins were visualized using the Gel Imaging System (Beijing Liuyi Factory, China) after reaction with ECL reagent (Solarbio). Quantitative data was obtained using the Gel-Pro-Analyzer software.

Caspase-3 activity assay

Caspase-3 activity was determined using a Caspase-3 Activity Assay Kit, according to the manufacturer's protocol. Briefly, cells were treated with Equol (20 μM and 40 μM) for 24 h, followed by lysing in lysis buffer on ice for 15 min and centrifugation at 16,000×*g* for 10 min. The protein concentration of the supernatant for each sample was measured by the Bradford's method. The reaction was started by adding caspase-3 substrate Ac-DEVD-pNA (10 μL). After incubation for 2 h at 37 °C, the cleavage of the substrate was detected at 405 nm using a microplate reader (ELX-800, BioTek). The activity of caspase-3 was expressed as changes in DEVDase activities.

Mitochondrial membrane potential (MMP) assay

The MMP of cells was analyzed using JC-1 staining. Briefly, cells were stained with JC-1 solution for 20 min at 37 °C. After being rinsed with JC-1 buffer for two times, the MMP of cells was assessed by fluorescence microscopy of JC-1-stained cells under an Olympus IX53 inverted microscope (OLYMPUS, Japan).

Label-free quantitative (LFQ) proteomics

Cells were lysed in lysis buffer containing protease inhibitor. After centrifuging at 14,100×*g* for 20 min, the supernatant was collected. The protein concentration was measured using the Bradford's method. The proteins from each sample were subjected to alkylation and digestion. LC–MS/MS analysis of tryptic peptides was conducted on a RIGOL L-3000 HPLC System (RIGOL, Beijing, China) coupled to a Thermo Scientific™ Orbitrap

Eclipse™ (ThermoFisher Scientific) via a Nanospray Flex™ (NSI) ion source (ThermoFisher Scientific). Peptides were separated using a gradient from 6 to 12% B in 13 min, then 12–30% B in 33 min and stepped up to 40% B in 7 min followed by a 10 min wash where solvent A was 0.1% formic acid in water and solvent B was 80% acetonitrile and 0.1% formic acid in water. MS spectra was collected in the Orbitrap mass analyzer (120,000 resolution, 350–1500 m/z range) with an automatic gain control target of 4×10^5 and a maximum ion injection time of 50 ms. All raw files were analyzed using the Proteome Discoverer suite (version 2.4, Thermo Fisher Scientific). The proteins with $Log_2FC > 1.0$ and P-value < 0.05 were considered to be differentially expressed proteins (DEPs). Gene Ontology (GO) analysis was conducted to obtain the functions of DEPs.

Molecular docking

The molecular structure of Equol (PubChem CID, 91,469) was retrieved from PubChem Compound (https://pubchem.ncbi.nlm.nih.gov/). The whole protein chain of TRIM21 (AlphaFold ID, AF-P19474-F1) was downloaded from the AlphaFold Protein Structure Database (https://alphafold.ebi.ac.uk/). Molecular docking was conducted to predict the binding affinities and modes of interaction between Equol and TRIM21 using an online analysis website (https://www.dockeasy.cn/).

RNA extraction and quantitative real-time PCR (qRT-PCR) analysis

Total RNA was extracted using the TriPure reagent (BioTeke, Beijing, China) according to the manufacturer's instructions. Final concentrations were determined using the NANO 2000 Spectrophotometer (ThermoFisher Scientific). The RNase inhibitor-treated RNA was reverse transcribed to cDNA using the BeyoRT II M-MLV reverse transcriptase (Beyotime). Amplification and detection were performed on the ExicyclerTM 96 Real-Time PCR System (BIONEER, Korea). The mRNA levels of the *TRIM21* and *ANXA2* genes were standardized against the expression of GAPDH. The primer sequences used for qRT-PCR are shown as follows: *TRIM21*, forward, 5′-CCCTTTGCTGGGTATGT-3′, reverse, 5′-AAACTCTGCGTGAATCCT-3′; *ANXA2*, forward, 5′-AAGGGTAGAAGAGCAGAG-3′, reverse, 5'-ATC CACTTGGGAACATC-3′.

Co-immunoprecipitation (Co-IP) assay

Cells were lysed in Cell lysis buffer for Western and IP (Beyotime). The lysates were centrifuged at 10,000×*g* for 5 min at 4 °C. The supernatants were incubated overnight with 1.0 μg of Goat Anti-Mouse IgG, Anti-TRIM21, or Anti-ANXA2 antibodies. The mixture was incubated for 2 h at 4 °C with 60 μL protein A/G agarose (Beyotime). The immunoprecipitated samples were washed 3 times with pre-cooled PBS buffer and then subjected to western blotting with the indicated antibodies including Anti-TRIM21, Anti-ANXA2, or Anti-Ubiquitin antibodies.

Immunofluorescence

The cells tested were fixed with 4% paraformaldehyde, and then followed a permeabilized procedure with 0.1% Triton X-100 solution (Beyotime). Proteins were blocked with 1% BSA (Sangon, Shanghai, China). Subsequently, slides were incubated with anti-TRIM21 and anti-ANXA2 overnight, followed by incubation with CY3-conjugated Goat Anti-Rabbit IgG and FITC-conjugated Goat Anti-Mouse IgG antibodies. Slides were washed with PBS, prior to counterstaining with 4′,6-diamidino-2-phenylindole (DAPI, Aladdin, Shanghai, China). Fluorescence microscopy was performed using a fluorescence microscope (Olympus, Japan).

β-catenin-driven transactivation assessed by dual-luciferase reporter gene assay

JEG-3 and Bewo cells were seeded into 12-well plates and then cultured for 24 h at 37 °C in a CO_2 incubator. Afterwards, TOPflash-luciferase plasmids (TOPflash-luc) purchased from Beyotime Biotechnology were co-transfected with Renilla-TK-luciferase reporter vectors (pRL-TK, Beyotime) into cells, using Lipofectamine 3000. Forty-eight hours after transfection, luciferase activities were measured using a Synergy™ H1 hybrid multi-mode microplate reader (BioTek). The activity of renilla luciferase was used as an internal control to normalize the firefly luciferase activity.

Nude mice subcutaneous xenograft model

Six to eight weeks-old balb/c nude mice were used in this study. Cultured logarithmic phase JEG-3 cells were collected and injected (5×10^6 cells per mouse) subcutaneously into the flank regions of mice. Then, mice were randomized into 2 groups and treated with vehicle (saline, i.g., QD) or Equol (20 mg/kg, i.g., QD). The tumor volume was assessed by caliper measurements every three days. At day 24 after the first administration, the tumors were collected, weighed, and then used for pathological analysis. All procedures complied with the Guide for the Care and Use of Laboratory Animals. The animal experiments were conducted with the approval of the Ethics Committee of Shengjing Hospital of China Medical University.

Immunohistochemistry

The 4% paraformaldehyde-fixed and paraffin-embedded tumor tissues were cut into 5 μm-thick sections. The

sections were deparaffinized in xylene and rehydrated through ethanol. Antigen retrieval was conducted by microwave heating for 10 min with sodium citrate buffer. Endogenous peroxidase activity was blocked by 3% H_2O_2 for 15 min at room temperature. Then, the sections were incubated at 4 °C overnight with primary antibodies against TRIM21 and ANXA2, followed by incubation for 1 h with the secondary antibody (HRP-conjugated Goat Anti-Rabbit IgG or Goat Anti-mouse IgG) at 37 °C. The reaction products were visualized using the Diaminobenzidine Kit. Finally, the sections were counterstained with hematoxylin and observed under an Olympus-BX53 microscope (OLYMPUS, Japan).

Statistics

The data represented in the results section are presented as means with error bars representing standard deviation (SD). All statistical analyses were conducted utilizing the GraphPad Prism version 8.0 software. Comparisons between two or more groups were analyzed by using Student's t-test, One-way ANOVA, or Two-way ANOVA. Levels of statistical significance were set at P value < 0.05.

Results

Metabolomic profiling of serum from normal subjects and patients with GTN

Firstly, we examined the variances in our data by OPLS-DA. Positive and negative ion data sets were treated separately. Parameters R2(Y) and Q2Y indicate the fitness and prediction ability, respectively. As shown in Fig. 1A, the OPLS-DA model showed a R2Y value of 0.837 and Q2Y value of 0.69 for the positive ion data while a R2Y value of 0.931 and Q2Y value of 0.812 for the negative ion data, suggesting that there is a clear segregation in the samples of GTN patients and healthy controls. Based on the VIP scores, Log_2FC, and P-value (Fig. 1B), 98 serum DMs in GTN patients relative to normal group were screened (Fig. 1C), in which 24 DMs were further characterized using reference compounds (Table 1). KEGG enrichment analysis showed that the significantly impacted signaling pathway in the serum metabolome was the Caffeine metabolism pathway (Fig. 1D). As shown in Fig. 1E, the top 3 DMs ranked by VIP score is 2-Deoxyguanosine, Aflatoxin B2 and Equol, respectively. To our knowledge, as a deoxyribonucleoside, studies on 2-Deoxyguanosine (VIP score, 6.223) mainly focus on DNA oxidative damage, such as aging [19]. Aflatoxin B2 (VIP score, 5.358) is a well-known carcinogenic risk factor [20]. Hence, Equol, an intestinal metabolite of the soy isoflavone daidzein, attracted our attention, partly because the high VIP score of 4.618 indicated its significant contribution to the class separation of normal and GTN samples, and partly because the extensive anticancer activity of daidzein. Meanwhile, multivariate receiver operating characteristics (ROC) curve was conducted to identify a diagnostic GTN-related metabolite signature. The ROC curve of Equol also showed a relatively good discrimination (AUC = 0.798, Fig. 1F). Taken together, we hypothesize that Equol may play a role in the development of GTN.

Equol inhibits choriocarcinoma cell proliferation but induces the apoptosis of choriocarcinoma cells

We first evaluated the cytotoxicity of Equol using CCK-8 assay. As shown in Fig. 2A, B, Equol showed a dose-dependent inhibitory effect on JEG-3 (IC_{50} = 150.366 μM) and Bewo (IC_{50} = 94.289 μM) cells. We further examined the effect of Equol at concentrations of 20 μM and 40 μM on cell cycle distribution of JEG-3 and Bewo cells (Fig. 2C). Equol treatment induced G1-phase cell cycle arrest, as evidenced by accumulation of a G1 phase population and decreases in a S phase population.

To detect cell apoptosis, cells were stained with Annexin V-FITC/PI and analyzed by flow cytometry. It was found that Equol triggered cell apoptosis (Fig. 3A). Western blot analyses of apoptosis-associated proteins showed that Equol up-regulated the expression of cleaved caspase-3, -7, and -9, as well as cleaved PARP (Figs. 3B and Supplementary Figure S1). Consistently, the activities of caspase-3 in the Equol-treated groups were obviously higher than those in the vehicle-treated group (Fig. 3C, D). Loss of MMP and Cyt C release from mitochondria into cytosol are key events during apoptosis. MMP was monitored to evaluate mitochondrial functions by using JC-1 staining. After Equol treatment, cells showed stronger green fluorescence and weaker red fluorescence (Fig. 3E), indicating that Equol results in the loss of MMP in JEG-3 and Bewo cells. Upon Equol treatment, there was a decrease in Cyt C in the mitochondrial fraction accompanied with an increase in that in the cytosolic fraction (Fig. 3F).

These results reveal the anti-proliferative and pro-apoptotic effects of Equol on choriocarcinoma cells.

Equol inhibits choriocarcinoma cell proliferation by up-regulating TRIM21

To screen the proteins regulated by Equol, LFQ proteomics were performed. Principal component analysis (PCA) exhibited that the Equol-treated group was separated from the vehicle-treated group (Fig. 4A). Based on the Log_2FC and P-value, 136 DEPs in the Equol group relative to the Veh. group were screened (Fig. 4B). The regulatory effects of Equol on protein degradation have been reported in a previous study [6]. GO enrichment analysis showed that six GO terms were associated with protein degradation, and twenty DEPs were enriched in the six GO terms (Fig. 4C). The twenty DEPs included eight

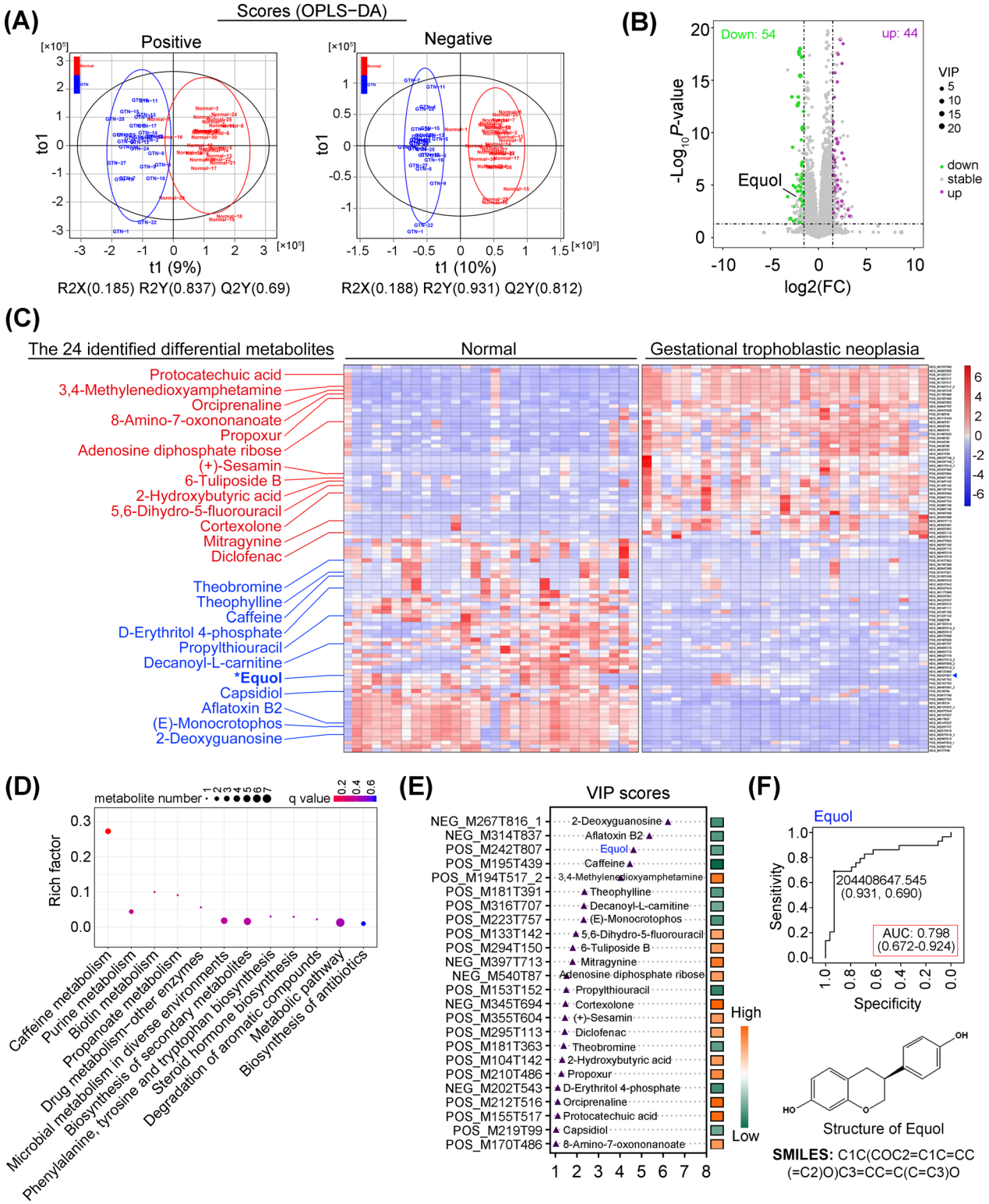

Fig. 1 Serum metabolomics reveals different metabolic profiles between normal subjects and patients with GTN. **A** The OPLS-DA score plot for GTN and normal. **B** Volcano plot of DMs. **C** Heatmap of DMs in normal and GTN groups. Log_2FC were calculated to show the differences in levels of metabolites. Those with $P < 0.05$, VIP ≥ 1, and $Log_2FC > 1.5$ were considered as the significant DMs between two groups. The threshold of VIP was set to 1. **D** KEGG enrichment analysis of the biological pathways of DMs. **E** The 24 identified DMs ranked by their contributions and shown as VIP scores. **F** A receiver operating characteristics (ROC) curve for Equol level prediction. *DMs* differential metabolites, *GTN* gestational trophoblastic neoplasia, *VIP* variable importance in the projection, *OPLS-DA* orthogonal projection to latent structures-discriminant analysis

Table 1 Twenty-four differential metabolites (DMs) identified between normal and gestational trophoblastic neoplasia (GTN) groups

No	RT/min	m/z	DMs	Formula	Log_2FC	*P*-value	VIP
NEG_M267T816_1	13.60	267.090	2-Deoxyguanosine	$C_{10}H_{13}N_5O_4$	−2.18	***	6.22
NEG_M314T837	13.95	314.077	Aflatoxin B2	$C_{17}H_{14}O_6$	−2.01	***	5.36
POS_M242T807	13.44	242.285	Equol	$C_{15}H_{14}O_3$	−1.90	***	4.62
POS_M195T439	7.32	195.088	Caffeine	$C_8H_{10}N_4O_2$	−2.91	*	4.45
POS_M194T517_2	8.61	194.116	3,4-Methylenedioxyamphetamine	$C_{11}H_{15}NO_2$	2.29	***	4.03
POS_M181T391	6.51	181.072	Theophylline	$C_7H_8N_4O_2$	−1.94	*	2.34
POS_M316T707	11.78	316.248	Decanoyl-L-carnitine	$C_{17}H_{33}NO_4$	−1.66	***	2.32
POS_M223T757	12.62	223.064	(E)-Monocrotophos	$C_7H_{14}NO_5P$	−2.10	***	2.30
POS_M133T142	2.37	133.032	5,6-Dihydro-5-fluorouracil	$C_4H_5FN_2O_2$	1.56	***	1.95
POS_M294T150	2.50	294.101	6-Tuliposide B	$C_{11}H_{18}O_9$	1.69	***	1.80
NEG_M397T713	11.88	397.203	Mitragynine	$C_{23}H_{30}N_2O_4$	2.27	***	1.79
NEG_M540T87	1.45	540.057	Adenosine diphosphate ribose	$C_{15}H_{23}N_5O_{14}P_2$	1.67	***	1.52
POS_M153T152	2.53	153.041	Propylthiouracil	$C_7H_{10}N_2OS$	−2.40	***	1.50
NEG_M345T694	11.57	345.144	Cortexolone	$C_{21}H_{30}O_4$	2.67	***	1.47
POS_M355T604	10.07	355.125	(+)-Sesamin	$C_{20}H_{18}O_6$	1.70	***	1.44
POS_M295T113	1.88	295.015	Diclofenac	$C_{14}H_{11}C_{l2}NO_2$	1.60	**	1.44
POS_M181T363	6.05	181.072	Theobromine	$C_7H_8N_4O_2$	−1.89	**	1.39
POS_M104T142	2.37	104.053	2-Hydroxybutyric acid	$C_4H_8O_3$	1.70	***	1.31
POS_M210T486	8.11	210.110	Propoxur	$C_{11}H_{15}NO_3$	1.98	***	1.27
NEG_M202T543	9.04	202.025	D-Erythritol 4-phosphate	$C_4H_{11}O_7P$	−2.22	*	1.11
POS_M212T516	8.61	212.126	Orciprenaline	$C_{11}H_{17}NO_3$	2.58	***	1.11
POS_M155T517	8.62	155.107	Protocatechuic acid	$C_7H_6O_4$	2.47	***	1.10
POS_M219T99	1.65	219.172	Capsidiol	$C_{15}H_{24}O_2$	−1.69	***	1.04
POS_M170T486	8.11	170.118	8-Amino-7-oxononanoate	$C_9H_{17}NO_3$	1.74	***	1.02

VIP variable importance in projection score of OPLS-DA model. Log_2fold changes (Log_2FC) were calculated to show the differences in levels of metabolites; Those with *P*-value < 0.05, VIP ≥ 1, and $Log_2FC > 1.5$ were considered as the significant DMs between two groups

up-regulated proteins and twelve down-regulated proteins (Fig. 4D). Seven proteins were enriched in more than one GO term related to protein degradation, including SNCA, PBK, TRIM21, NSFL1C, VPS28, STAM2, and HSPA1B (Fig. 4C). TRIM21 functions as a E3 ligase and negatively regulates protein stability [21]. Molecular docking analysis showed that Equol interacted with the amino acid residues of TRIM21 through visible hydrogen bonds and pi stacking (Fig. 4E). The low binding energy of −6.939 kcal/mol indicated the highly stable binding between them [22]. Western blot analysis of TRIM21 confirmed the up-regulated protein levels of TRIM21 induced by Equol (Fig. 4F).

To explore the involvement of TRIM21 in Equol-induced effects on choriocarcinoma cells, choriocarcinoma cell lines JEG-3 and Bewo were transfected with siTRIM21 that had been verified to effectively silence TRIM21 (Fig. 5A) and treated with Equol for 24 h at 48 h after cell transfection. As shown in Fig. 5B, C, TRIM21 silencing reversed Equol-induced decreases in cell proliferation and increases in cell apoptosis, indicating that Equol has regulatory effects on choriocarcinoma cell proliferation and apoptosis via TRIM21.

Equol promotes ANXA2 degradation through TRIM21-mediated ubiquitination of ANXA2

The protein–protein interaction (PPI) information from the public database BioGRID (https://thebiogrid.org/) showed that ANXA2 could interact with TRIM21 (Fig. 6A). Immunofluoresce staining revealed co-localization of TRIM21 and ANXA2 proteins in JEG-3 and Bewo cells (Fig. 6B). Co-IP assays further confirmed the interaction between TRIM21 and ANXA2 proteins in JEG-3 and Bewo cells (Fig. 6C). We next observed down-regulation of ANXA2 in Equol-treated JEG-3 and Bewo cells, however, the down-regulation was inhibited by TRIM21 silencing (Fig. 6D). The result suggests that Equol reduces ANXA2 protein expression by up-regulating TRIM21. TRIM21 silencing reduced the ubiquitination of ANXA2, but Equol treatment promoted its ubiquitination (Fig. 6E, F). Moreover, MG132, a proteasome inhibitor, could reversed Equol-induced down-regulations in ANXA2 protein expression (Fig. 6G). These findings imply that the Equol-induced ANXA2 degradation is mediated by TRIM21 in a proteasome-dependent manner.

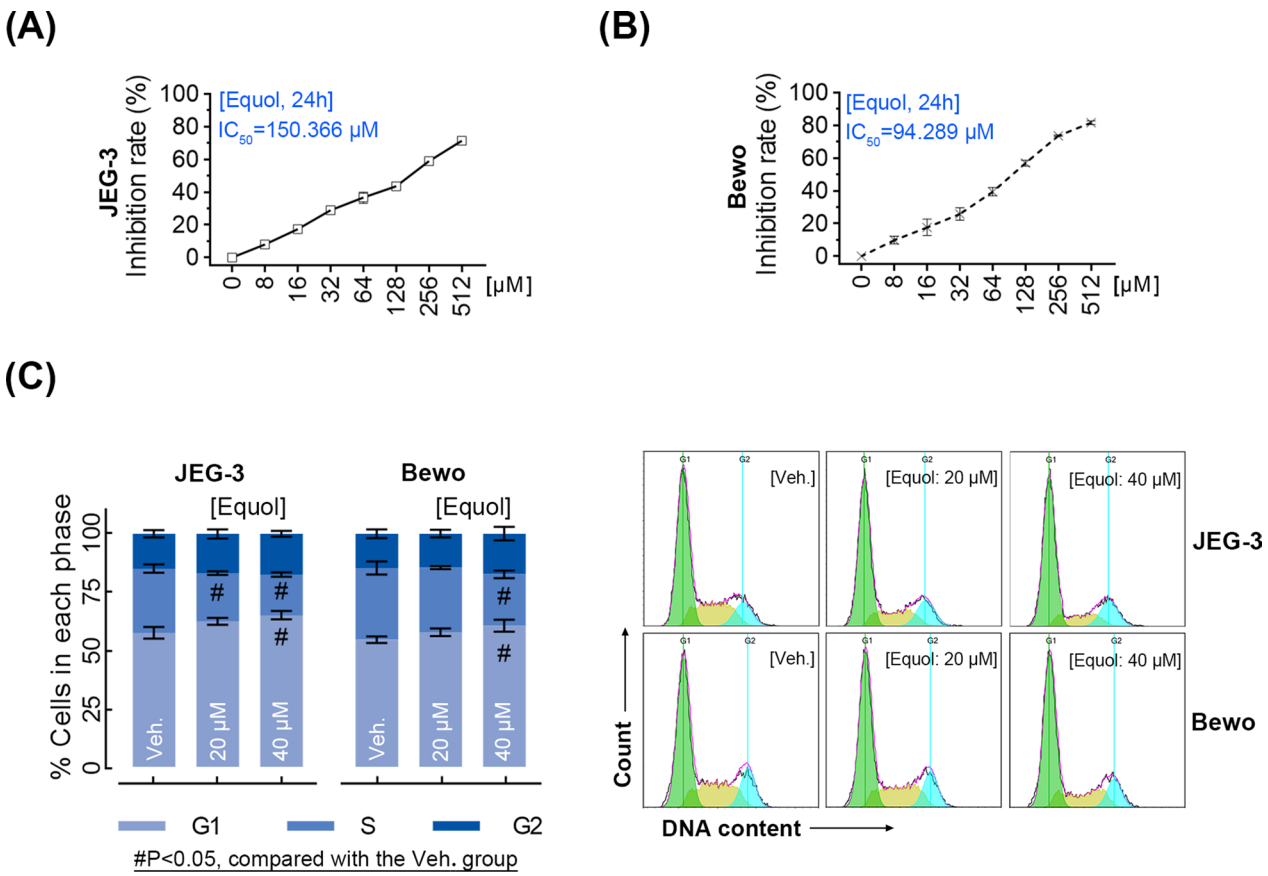

Fig. 2 Effects of Equol on choriocarcinoma cell proliferation and cell cycle. JEG-3 and Bewo cells were treated with different concentrations of Equol for 24 h. **A** and **B** CCK-8 assays were performed to detect the growth inhibition of cells. After treatment with Equol (20 or 40 μM) or vehicle for 24 h, **C** cell cycle distribution was determined by flow cytometry. *Veh.* vehicle

Equol-triggered effects on choriocarcinoma cell proliferation and apoptosis and β-catenin activation are TRIM21-ANXA2 dependent

The siANXA2 that had been confirmed to effectively knock down ANXA2 (Fig. 7A) was co-transfected with siTRIM21 into choriocarcinoma cell lines JEG-3 and Bewo and treated with Equol for 24 h at 48 h after cell transfection. As shown in Fig. 7B, C, ANXA2 silencing restored the increases in proliferation and the decreases in apoptosis of Equol-treated cells induced by siTRIM21, indicating that Equol depends on the TRIM21-ANXA2 axis to regulate choriocarcinoma cell proliferation and apoptosis.

ANXA2 has been reported to exert a pro-tumor effect via β-catenin [23]. We found that Equol could inhibit β-catenin-mediated transcription activation (Fig. 8A). The inhibition of β-catenin-mediated transcription activation resulted from Equol treatment was reversed by TRIM21 silencing (Fig. 8B). Furthermore, ANXA2 silencing suppressed the siTRIM21-induced increases in β-catenin-mediated transcription activation (Fig. 8C). The data demonstrate that Equol negatively regulates β-catenin activation via the TRIM21-ANXA2 axis (Fig. 8D).

Equol inhibits JEG-3 cell growth in vivo

We subsequently assessed whether Equol could inhibit tumorigenesis in vivo by using the JEG-3 xenograft mouse model. Macroscopic evaluation of tumor clearly showed that the tumor burden in control mice was significantly higher than that in mice under Equol treatment (Fig. 9A). In line with our in vitro results, it was found that Equol also up-regulated TRIM21 expression and down-regulated ANXA2 expression in tumor tissues (Fig. 9B, C). All these findings suggest that Equol can effectively the growth of JEG-3-derived xenograft tumors in vivo.

Discussion

The results of our metabolomic study highlighted that the level of Equol in GTN serum samples was significantly lower than that in normal samples, implying that

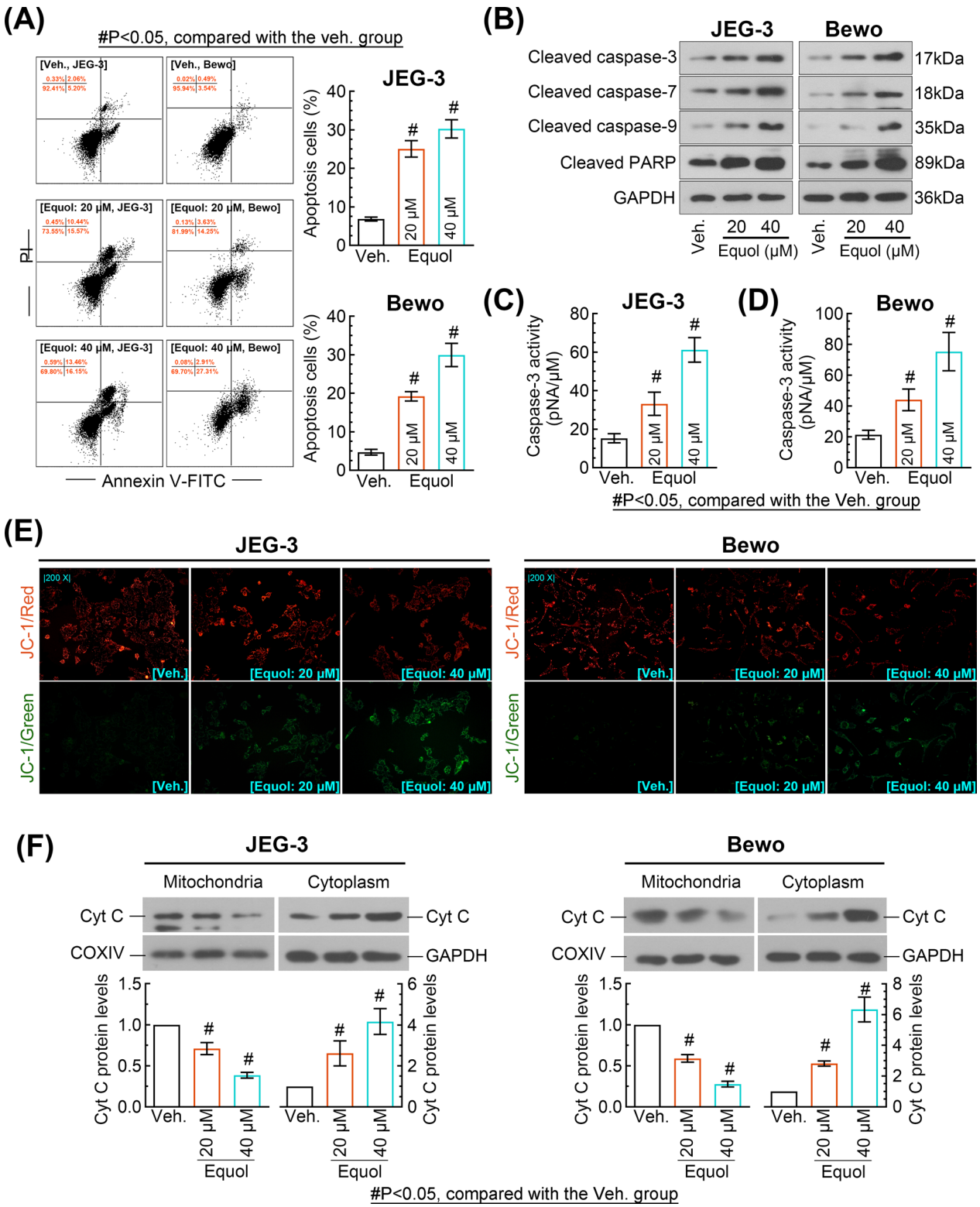

Fig. 3 Effects of Equol on choriocarcinoma cell apoptosis. JEG-3 and Bewo cells were treated with Equol (20 or 40 μM) or vehicle for 24 h, and then subjected to **A** Annexin V-FITC/PI apoptosis assays. **B** The expression of apoptosis-related proteins, including cleaved caspase-3, cleaved caspase-7, cleaved caspase-9, and cleaved PARP, was determined by western blot. **C** and **D** The activity of caspase-3 was measured. **E** JC-1 staining was performed to evaluate the mitochondria membrane potential of cells. **F** Cytoplasm and mitochondria fraction were subjected to western blot to detect Cyt C. *Veh* vehicle, *Cyt C* cytochrome C

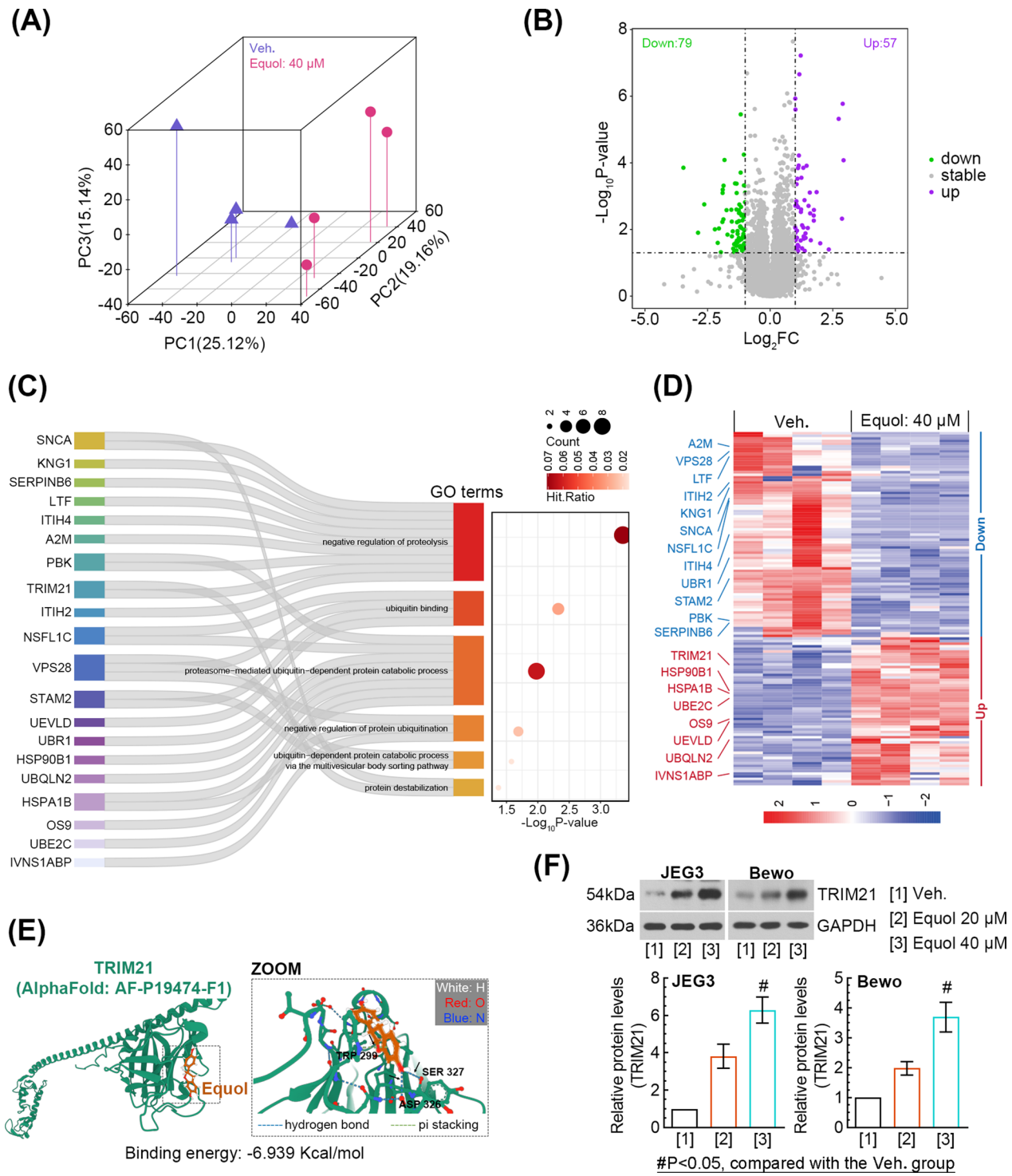

Fig. 4 Screening of the proteins regulated by Equol in choriocarcinoma cells. **A** The PCA plot for the similarity assessment of samples from the Veh. group and the Equol group. **B** The volcano plot showing the DEPs in the Equol group when compared with the Veh. group. The proteins with $P < 0.05$ and $Log_2FC > 1$ were considered as the significant DEPs between two groups. **C** The sankey diagram combined with a bubble diagram visualized the significantly enriched GO terms associated with protein degradation and the proteins annotated within. **D** The heatmap visualized the expression patterns of DEPs, and the proteins enriched in the GO terms associated with protein degradation were highlighted. **E** The binding mode of Equol to TRIM21 by molecule docking. **F** JEG-3 and Bewo cells were treated with Equol (20 or 40 μM) or vehicle for 24 h. The expression of TRIM21 was measured by western blot. *PCA* principal component analysis, *Veh.* vehicle

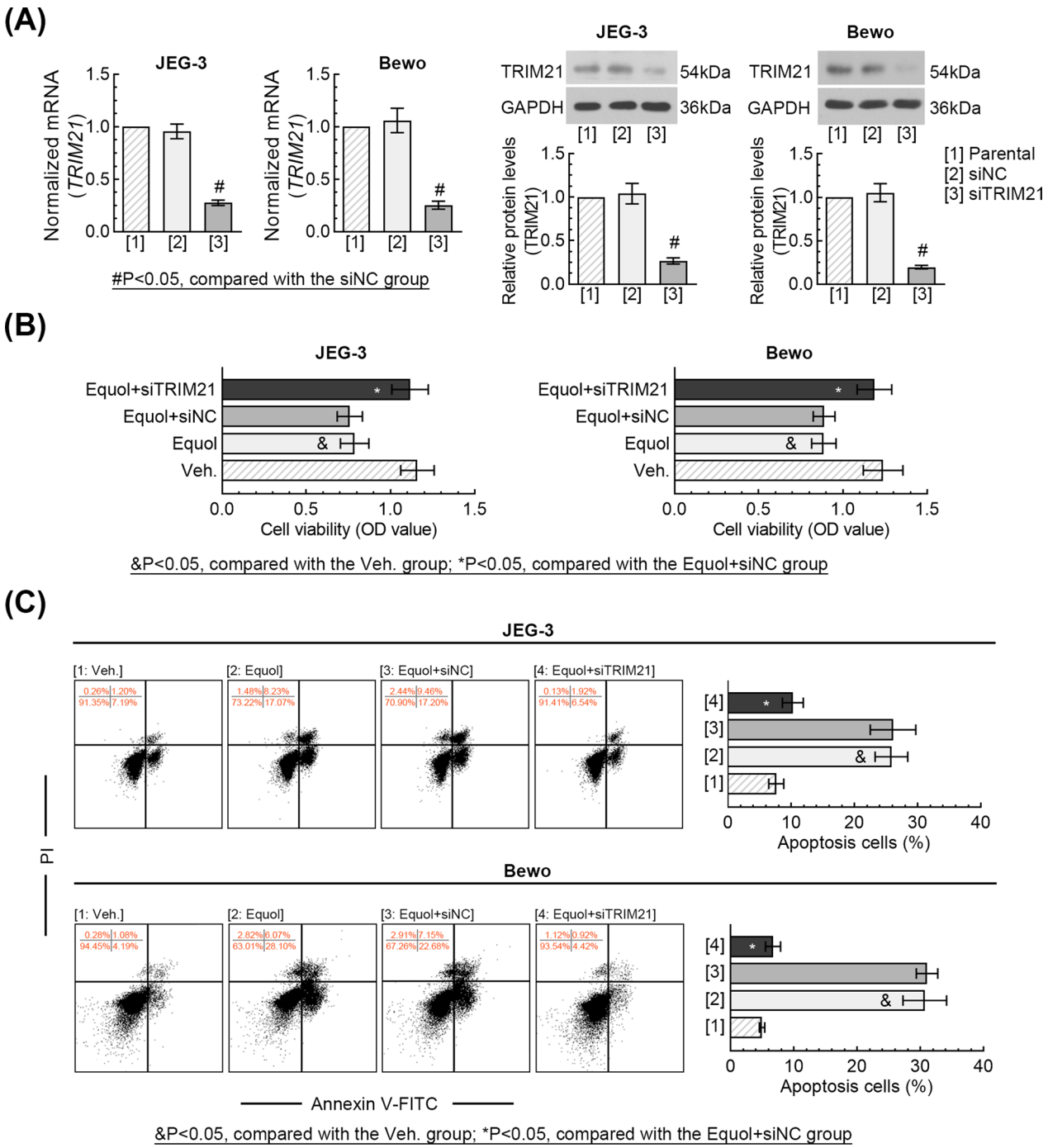

Fig. 5 Roles of TRIM21 in the effect of Equol on choriocarcinoma cell proliferation and apoptosis. **A** JEG-3 and Bewo cells were transfected with siTRIM21 or siNC for 48 h. The expression levels of TRIM21 mRNA and protein were measured by qRT-PCR and western blot. At 48 h after cell transfection, the cells were treated with 40 μM Equol for 24 h. **B** Cell viability was detected by CCK-8 assay. **(C)** Cell apoptosis was determined by flow cytometry. *Veh.* vehicle

Equol may play a role in the development of GTN. An in vitro study using daidzein to incubate isolated trophoblast cells of term placentas suggested that daidzein exposure effectively reduced the production of human chorionic gondaotropin in human term trophoblasts [24]. It is well-known that choriocarcinoma is characterized by high levels of human chorionic gondaotropin. Besides, Zheng et al. suggested that daidzein could inhibit

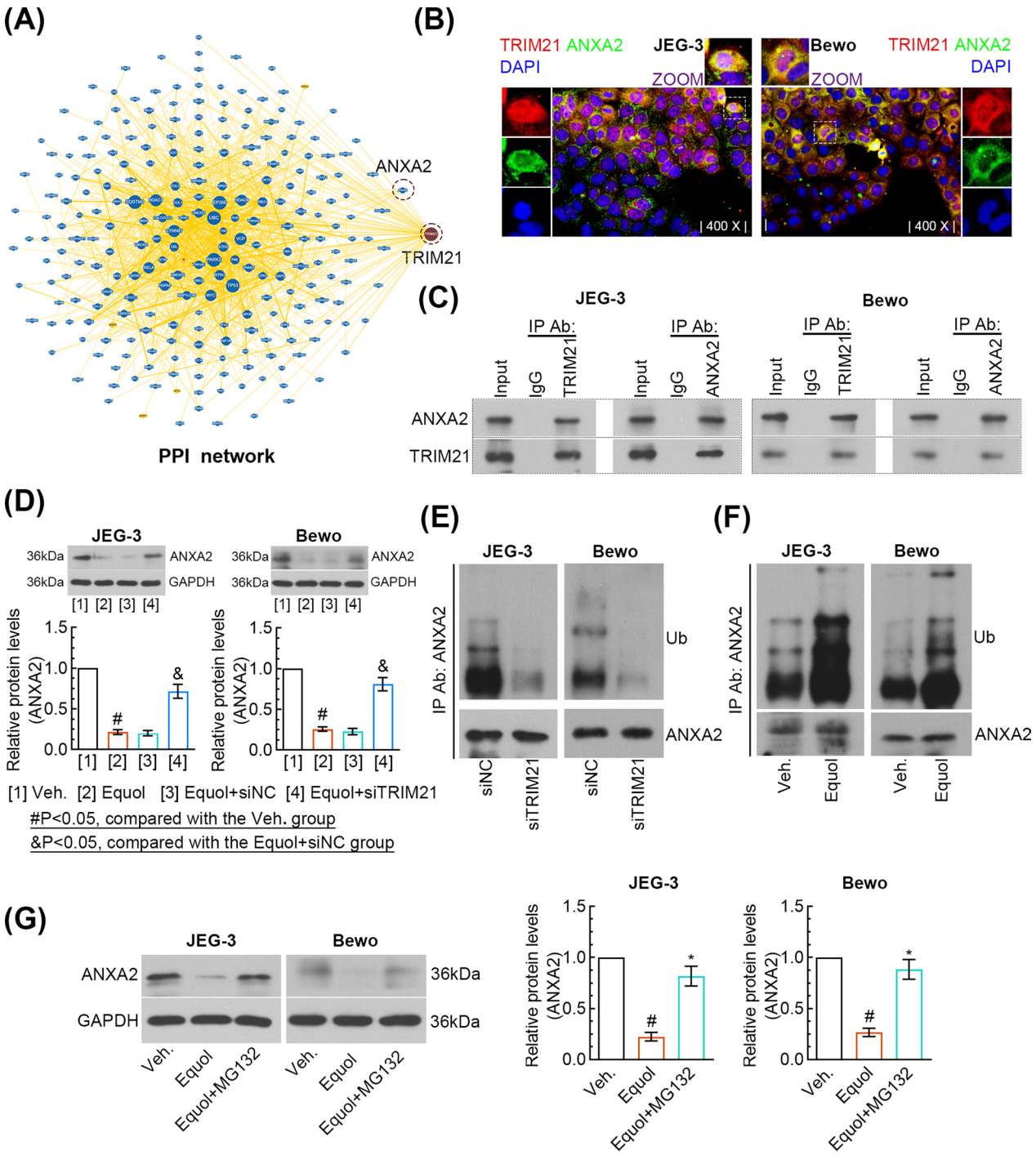

Fig. 6 Effects of Equol and TRIM21 on the ubiquitination of AXNA2. **A** The PPI network showing the proteins interacted with TRIM21. **B** Double immunofluorescence staining of TRIM21 (red) and AXNA2 (green) in JEG-3 and Bewo cells. **C** Co-immunoprecipitation of TRIM21 with AXNA2 in JEG-3 and Bewo cells. **D** JEG-3 and Bewo cells were transfected with siTRIM21 or siNC for 48 h, and then treated with 40 μM Equol for 24 h. The expression of AXNA2 was measured by western blot. **E** JEG-3 and Bewo cells were transfected with siTRIM21 or siNC for 48 h, and 12-h treatment with MG132 (10 μM) was subjected before cell harvesting. **F** JEG-3 and Bewo cells were treated with 40 μM Equol for 24 h, and 12-h treatment with MG132 (10 μM) was subjected before cell harvesting. **E** and **F** The ubiquitination of AXNA2 was detected by co-immunoprecipitation of AXNA2 with ubiquitin. **G** JEG-3 and Bewo c ells were treated with 40 μM Equol and 10 μM MG132 for 24 h. Western blot analysis of AXNA2 was performed. *Veh.* Vehicle, *Ub* ubiquitin

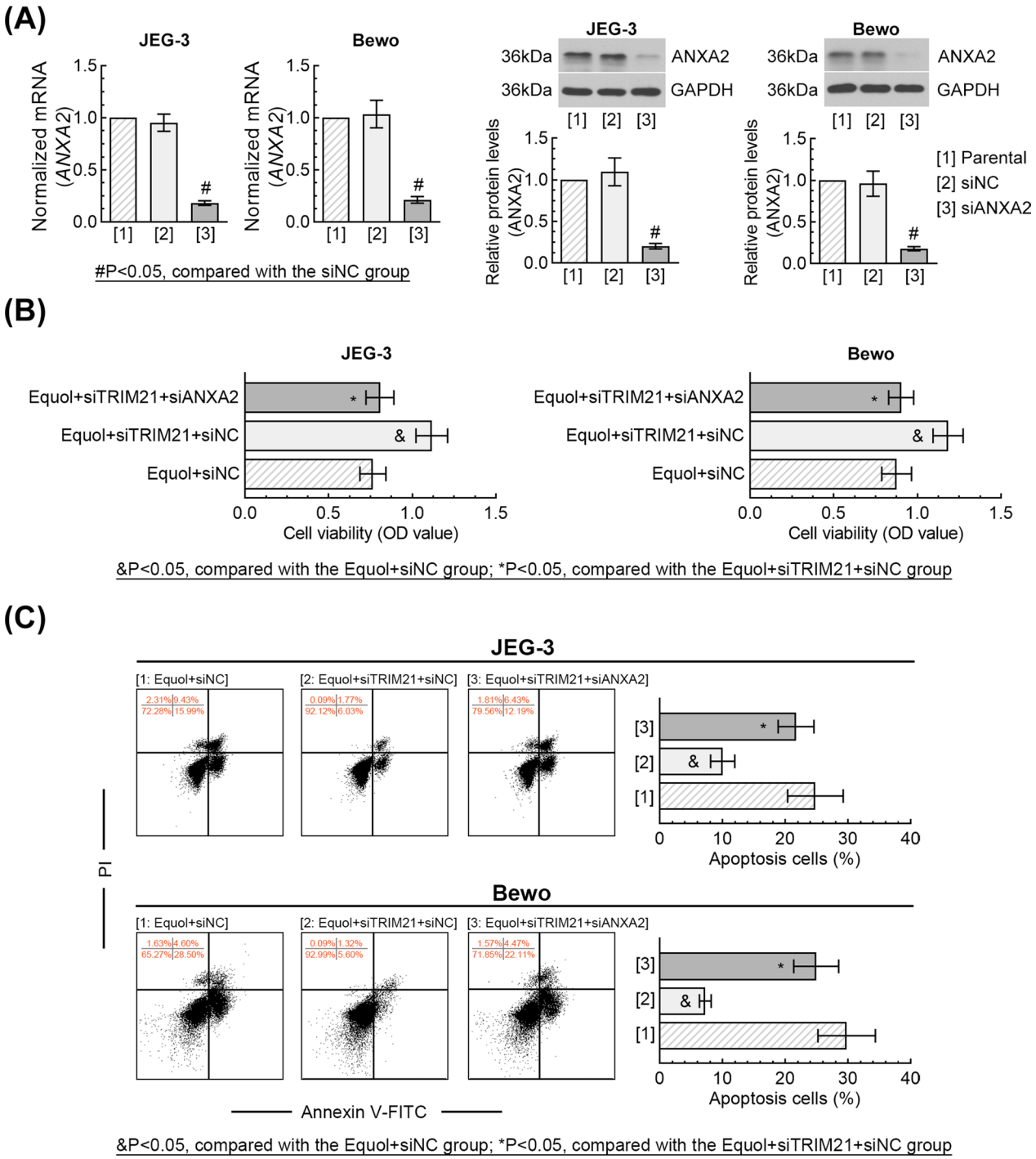

Fig. 7 Roles of ANXA2 in the effect of TRIM21 on the proliferation and apoptosis of Equol-treated choriocarcinoma cells. **A** JEG-3 and Bewo cells were transfected with siANXA2 or siNC for 48 h. The expression levels of ANXA2 mRNA and protein were measured by qRT-PCR and western blot. JEG-3 and Bewo cells were co-transfected with siTRIM21 and siANXA2 for 48 h, and then treated with 40 μM Equol for 24 h. **B** Cell viability was detected by CCK-8 assay. **C** Cell apoptosis was determined by flow cytometry. *Veh.* vehicle

choriocarcinoma cell proliferation both in vitro and in vivo [25]. However, few studies regarding the effect of daidzein metabolites, such as Equol, on choriocarcinoma have been published. Herein, experiments performed on JEG-3 and Bewo cells showed that Equol effectively inhibited cell proliferation, triggered arrest at the G1 phase of

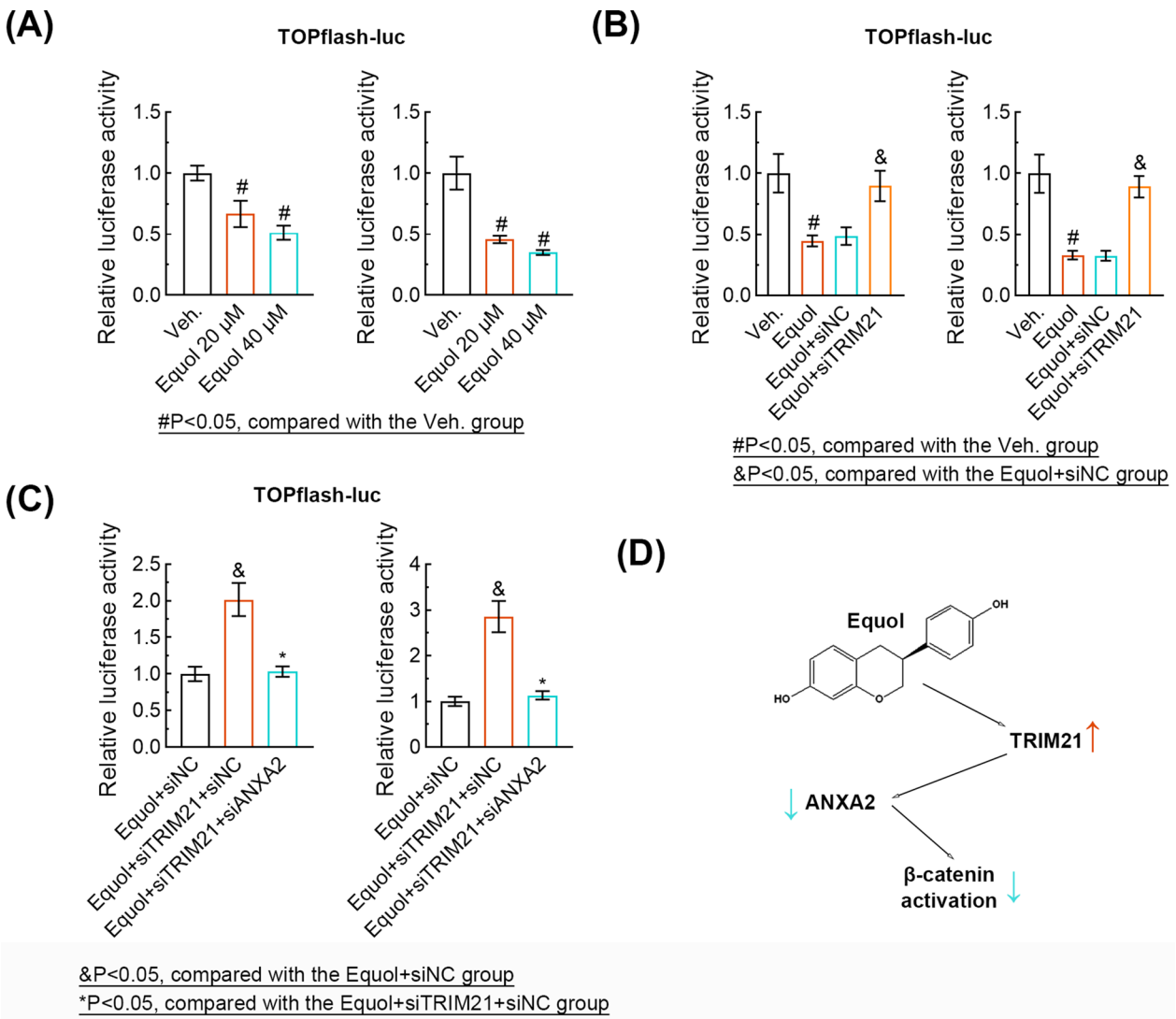

Fig. 8 Roles of TRIM21 and AXNA2 in Equol-induced effects on β-catenin activation. **A** JEG-3 and Bewo cells were co-transfected with TOPflash-luc and pRL-TK and treated with 20 or 40 μM Equol for 48 h. **B** The siTRIM21 or siNC was co-transfected with TOPflash-luc and pRL-TK into JEG-3 and Bewo cells for 48 h, and then the cells treated with 40 μM Equol for 24 h. **C** JEG-3 and Bewo cells were co-transfected with siTRIM21, siANXA2, TOPflash-luc, and pRL-TK for 48 h, and then treated with 40 μM Equol for 24 h. **A**–**C** The relative activity of luciferase was measured. *Veh.* vehicle. **D** Schematic illustration of the mechanism of β-catenin activation regulated by Equol

cell cycles, and promoted cell apoptosis. Mechanistically, we emphasized that Equol may lead to the inhibition of cell proliferation and cell apoptosis through the TRIM21-ANXA2-β-catenin axis. In addition, in vivo study demonstrated that Equol could suppress the tumor xenograft growth in mice, suggesting the potential of Equol in the treatment of choriocarcinoma.

Several studies have revealed that Equol effectively inhibits proliferation of a variety of human tumor cells, such as human gastric carcinoma cells (MGC-803) [11, 26], human prostate cancer cells (LNCaP and 22Rv1) [6], and human breast cancer cells (MCF-7) [27]. The present study is the first to demonstrated that Equol (> 20 μM) could inhibit the growth of choriocarcinoma cells. The execution phase of apoptosis involves the activation of a series of caspases that play a central role in apoptosis [28]. For example, initiator caspases like caspase-9 that are primarily responsible for the initiation of the apoptotic pathway and effector caspases such as caspase-3 and -7 which are responsible in the actual cleavage of cellular components during apoptosis [29, 30]. Accordingly, the increases in the levels of cleaved caspase-3, -7, and -9, as well as cleaved PARP suggest that Equol-induced apoptosis may be mediated

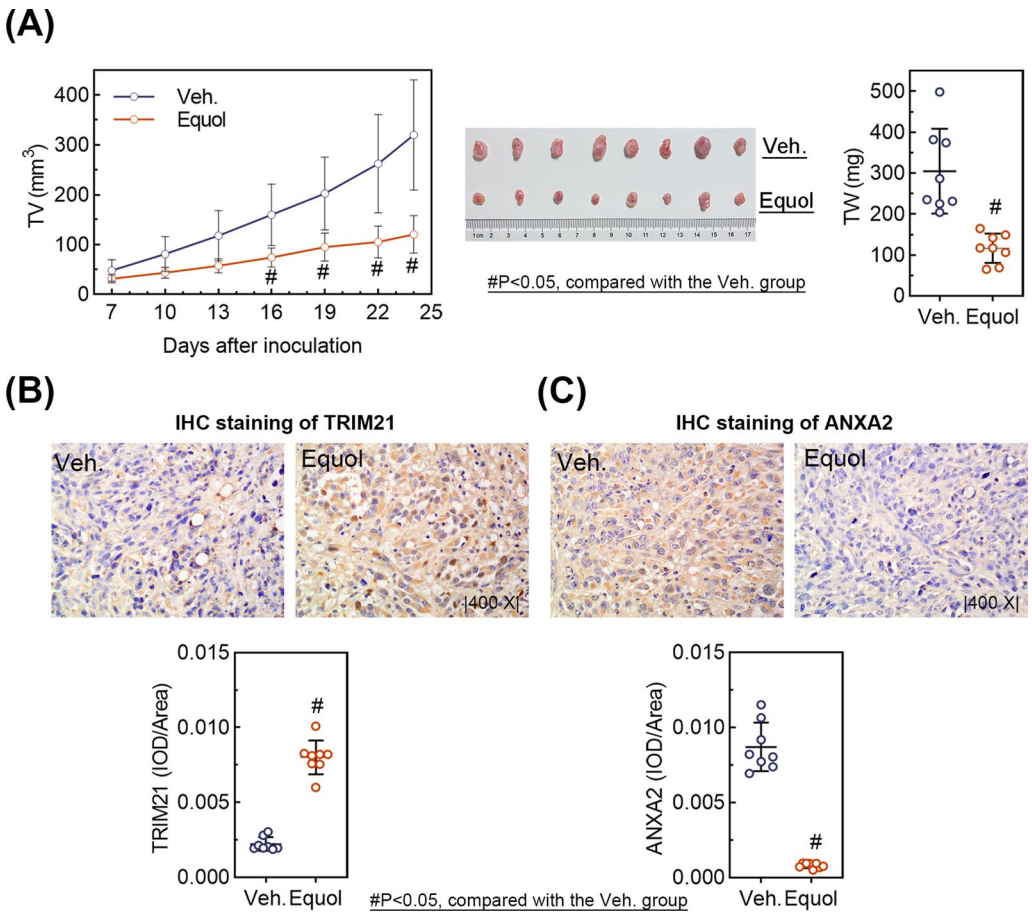

Fig. 9 Equol inhibits tumor growth in vivo. Babl/c nude mice bearing JEG-3-derived tumor xenografts were administrated with Equol (20 mg/kg) or vehicle once a day by gavage. **A** Tumor volumes, tumor pictures, and tumor weight (TW) results showed that Equol exerted an inhibitory effect on the growth of the JEG-3-derived tumor xenografts. Tumor volume (TV) = $0.5 \times a \times b^2$; a: the longest diameter; b: the shortest diameter. **B** and **C** Immunohistochemical staining analysis of tumor tissues was performed using anti-TRIM21 and anti-ANXA2 antibodies. *Veh.* vehicle

by caspases activation. In addition, daidzein induces apoptosis via the mitochondrial apoptotic pathway has been confirmed in many cancer types, including choriocarcinoma [31, 32]. Consistently, here we found that Equol treatment compromised mitochondrial function as evidenced by the release of Cyt C from mitochondria into cytosol and the loss of MMP in choriocarcinoma cells. Thus, our data indicate that the mitochondrial-dependent pathway contributes to the apoptosis of choriocarcinoma cells induced by Equol.

Emerging evidence has demonstrated that TRIM21 can be regulated by drugs such as sorafenib [33] and vilazodone [34]. TRIM21 was up-regulated by sorafenib and mediated the synergistic effect of sorafenib and olaparib on breast cancer cells [33]. TRIM21 was identified as a direct target of vilazodone that promoted the interaction between TRIM21 and its substrate MST2 instead of TRIM21 expression in colorectal cancer cells [34]. In the present study, increases in TRIM21 expression was observed in the Equol-treated choriocarcinoma cells by performing LFQ proteomics. We also observed increased expression of TRIM21 in xenograft tumors derived from choriocarcinoma cells by Equol administration. Molecule docking predicted that there may be a potential binding of Equol to TRIM21. We hypothesized that TRIM21 may be regulated by Equol via a direct or indirect way.

The ubiquitin–proteasome pathway was the main pathway mediating degradation of most of the intracellular proteins. A serial of enzymes, including the ubiquitin-activating enzyme E1, the ubiquitin-conjugating enzyme E2, and a ubiquitin ligase E3, involves in the progress of ubiquitination. As a E3 ligase, TRIM21 has been reported to modulate ubiquitination of multiple proteins [17, 35–37]. The present study confirmed the regulation of ANXA2 ubiquitination by TRIM21 in choriocarcinoma cells. Moreover, the Equol-induced down-regulation of ANXA2 was TRIM21-dependent. We speculated TRIM21 may mediate the

proteasome-dependent degradation of ANXA2 induced by Equol. The tumor-promoting roles of ANXA2 have confirmed in many types of cancer [38–41]. The results in the present study suggested that Equol induced effects on choriocarcinoma cells by promoting TRIM21-induced ubiquitination of ANXA2, which highlighted the importance of TRIM21-ANXA2 axis in anti-tumor effects induced by Equol.

β-catenin plays a vital role in controlling physiological and pathological processes. Activation of β-catenin promotes the transcription of genes associated with cell cycle, including cyclin D1 and c-myc, and thereby modulates cell cycle distribution and cell proliferation [42, 43]. β-catenin inhibition was found to cause a decrease in choriocarcinoma cell proliferation [44]. Notably, AXNA2 can promote the nuclear translocation of β-catenin, leading to β-catenin activation [45]. The present study uncovered Equol inhibited β-catenin activation through TRIM21-mediated reduction of AXNA2. Given the role of β-catenin in cancer cell proliferation and apoptosis, it is hypothesized that the Equol-induced increases in cell proliferation may be attributed to inhibition of β-catenin activation.

Conclusions

In summary, Equol exhibited anti-tumor effects on choriocarcinoma cells through inducing cell cycle arrest at the G1 phase and promoting cell apoptosis, which may be mediated by the TRIM21-ANXA2-β-catenin axis. Our work demonstrated that Equol may have a potential to inhibit the progression of choriocarcinoma. Besides, Paunović et al. has confirmed anti-proliferative potential of resveratrol on JEG-3 cell lines [46]. The combination of resveratrol and Equol has a synergistic effect on prostate cancer cell lines [47]. Whether the combination also shows synergy in choriocarcinoma cells remains to be explored.

Abbreviations

GTN	Gestational trophoblastic neoplasia
DMs	Differential metabolites
LFQ	Label-free quantitative
DEPs	Differentially expressed proteins
GO	Gene ontology
TRIM21	Tripartite motif containing 21
ANXA2	Annexin A2
Cleaved PARP	Cleaved poly (ADP-ribose) polymerase
Cyt C	Cytochrome C
OPLS-DA	Orthogonal projection to latent structures-discriminant analysis
VIP	Variable importance in projection
Log_2FC	Log_2fold changes
KEGG	Kyoto Encyclopedia of Genes and Genomes
SiRNA	Small interference RNA
PMSF	Phenylmethylsulfonyl fluoride
SDS-PAGE	Sodium dodecyl sulfate polyacrylamide gel electrophoresis
MMP	Mitochondrial membrane potential
qRT-PCR	Quantitative real-time PCR
Co-IP	Co-immunoprecipitation
i.g.	Intragastrical administration
SD	Standard deviation
ROC	Receiver operating characteristics
PCA	Principal component analysis

Supplementary Information

The online version contains supplementary material available at https://doi.org/10.1186/s13062-024-00519-5.

Supplementary Material 1. Figure S1. Quantification of the relative protein expression of apoptosis-related proteins in Figure 3B. (A and B) The expression levels of cleaved caspase-3, cleaved caspase-7, cleaved caspase-9, and cleaved PARP in JEG-3 and Bewo cells. Veh.: vehicle.

Acknowledgements

Not applicable.

Author contributions

Xiaomei Liu and Xiaoxin Ma: Conceptualization, Writing—original draft, and Writing—review and editing; Xiaomei Liu, Zihao Wang, Qianxue Wei, and Yang Song: Data curation, Investigation, Validation, and Formal analysis. All authors read and approved the final paper.

Funding

This research did not receive any specific grant from funding agencies in the public, commercial, or not-for-profit sectors.

Availability of data and materials

All data generated or analyzed during this study will be made available on request.

Declarations

Ethics approval and consent to participate

All experiments involving human samples and animals were conducted with the approval of the Ethics Committee of Shengjing Hospital of China Medical University for Ethical Review (Human study No. 2023PS012K; Animal study No. 2023PS011K). The informed consent was obtained from all participants.

Consent for publication

Not applicable.

Competing interests

The authors declare no competing interests.

Author details

[1]Department of Obstetrics and Gynecology, Shengjing Hospital of China Medical University, 36 Sanhao Street, Heping District, Shenyang 110004, Liaoning, China.

Received: 10 June 2024 Accepted: 8 August 2024
Published online: 06 September 2024

References

1. Shaaban AM, Rezvani M, Haroun RR, et al. Gestational trophoblastic disease: clinical and imaging features. Radiograph: Rev Pub Radiol Soc North Am, Inc. 2017;37:681–700.
2. Soper JT. Gestational trophoblastic disease: current evaluation and management. Obstet Gynecol. 2021;137:355–70.
3. Abu-Rustum NR, Yashar CM, Bean S, et al. Gestational trophoblastic neoplasia, version 2.2019, NCCN Clinical practice guidelines in oncology. J Natl Compr Cancer Netw: JNCCN. 2019;17:1374–91.
4. Muthyala RS, Ju YH, Sheng S, et al. Equol, a natural estrogenic metabolite from soy isoflavones: convenient preparation and resolution of R- and

S-equols and their differing binding and biological activity through estrogen receptors alpha and beta. Bioorg Med Chem. 2004;12:1559–67.
5. Setchell KD, Borriello SP, Hulme P, Kirk DN, Axelson M. Nonsteroidal estrogens of dietary origin: possible roles in hormone-dependent disease. Am J Clin Nutr. 1984;40:569–78.
6. Itsumi M, Shiota M, Takeuchi A, et al. Equol inhibits prostate cancer growth through degradation of androgen receptor by S-phase kinase-associated protein 2. Cancer Sci. 2016;107:1022–8.
7. Hod R, Maniam S, Mohd Nor NH. A systematic review of the effects of equol (soy metabolite) on breast cancer. Molecules (Basel, Switzerland). 2021;26:1105.
8. Lampe JW. Emerging research on equol and cancer. J Nutr. 2010;140:1369s–72s.
9. Yamashita S, Lin I, Oka C, et al. Soy isoflavone metabolite equol inhibits cancer cell proliferation in a PAP associated domain containing 5-dependent and an estrogen receptor-independent manner. J Nutr Biochem. 2022;100:108910.
10. Kim EY, Shin JY, Park YJ, Kim AK. Equol induces mitochondria-mediated apoptosis of human cervical cancer cells. Anticancer Res. 2014;34:4985–92.
11. Yang Z, Zhao Y, Yao Y, et al. Equol induces mitochondria-dependent apoptosis in human gastric cancer cells via the sustained activation of ERK1/2 pathway. Mol Cells. 2016;39:742–9.
12. Jones EL, Laidlaw SM, Dustin LB. TRIM21/Ro52: roles in innate immunity and autoimmune disease. Front Immunol. 2021;12:738473.
13. Ozato K, Shin DM, Chang TH, Morse HC 3rd. TRIM family proteins and their emerging roles in innate immunity. Nat Rev Immunol. 2008;8:849–60.
14. Chu Y, Yang X. SUMO E3 ligase activity of TRIM proteins. Oncogene. 2011;30:1108–16.
15. Ben-Chetrit E, Chan EK, Sullivan KF, Tan EM. A 52-kD protein is a novel component of the SS-A/Ro antigenic particle. J Exp Med. 1988;167:1560–71.
16. Kara-Ali GH, Cano L, Dion S, et al. Trim21 deficiency in mice increases HCC carcinogenesis in a NASH context and is associated with immune checkpoint upregulation. Int J Cancer. 2024;154:1999–2013.
17. Chen X, Yong H, Chen M, et al. TRIM21 attenuates renal carcinoma lipogenesis and malignancy by regulating SREBF1 protein stability. J Exp Clin Cancer Res: CR. 2023;42:34.
18. Zhang R, Shen Y, Zhang Q, et al. TRIM21-mediated Sohlh2 ubiquitination suppresses M2 macrophage polarization and progression of triple-negative breast cancer. Cell Death Dis. 2023;14:850.
19. Fleming AM, Muller JG, Ji I, Burrows CJ. Characterization of 2'-deoxyguanosine oxidation products observed in the Fenton-like system Cu(II)/H2O2/reductant in nucleoside and oligodeoxynucleotide contexts. Org Biomol Chem. 2011;9:3338–48.
20. Aydın M, Aydın S, Bacanlı M, Başaran N. Aflatoxin levels in chronic hepatitis B patients with cirrhosis or hepatocellular carcinoma in Balıkesir. Turk J Viral Hepat. 2015;22:926–35.
21. Zhang L, Li Q, Yang J, et al. Cytosolic TGM2 promotes malignant progression in gastric cancer by suppressing the TRIM21-mediated ubiquitination/degradation of STAT1 in a GTP binding-dependent modality. Cancer Commun (Lond, Engl). 2023;43:123–49.
22. Ferreira LG, Dos Santos RN, Oliva G, Andricopulo AD. Molecular docking and structure-based drug design strategies. Molecules (Basel, Switzerland). 2015;20:13384–421.
23. Yan X, Zhang D, Wu W, et al. Mesenchymal stem cells promote hepatocarcinogenesis via lncRNA-MUF interaction with ANXA2 and miR-34a. Can Res. 2017;77:6704–16.
24. Jeschke U, Briese V, Richter DU, et al. Effects of phytoestrogens genistein and daidzein on production of human chorionic gonadotropin in term trophoblast cells in vitro. Gynecol Endocrinol: Off J Int Soc Gynecol Endocrinol. 2005;21:180–4.
25. Zheng W, Sun R, Yang L, et al. Daidzein inhibits choriocarcinoma proliferation by arresting cell cycle at G1 phase through suppressing ERK pathway in vitro and in vivo. Oncol Rep. 2017;38:2518–24.
26. Yang ZP, Zhao Y, Huang F, et al. Equol inhibits proliferation of human gastric carcinoma cells via modulating Akt pathway. World J Gastroenterol. 2015;21:10385–99.
27. Zhang J, Ren L, Yu M, et al. S-equol inhibits proliferation and promotes apoptosis of human breast cancer MCF-7 cells via regulating miR-10a-5p and PI3K/AKT pathway. Arch Biochem Biophys. 2019;672:108064.
28. Carneiro BA, El-Deiry WS. Targeting apoptosis in cancer therapy. Nat Rev Clin Oncol. 2020;17:395–417.
29. Wong RS. Apoptosis in cancer: from pathogenesis to treatment. J Exp Clin Cancer Res: CR. 2011;30:87.
30. Fink SL, Cookson BT. Apoptosis, pyroptosis, and necrosis: mechanistic description of dead and dying eukaryotic cells. Infect Immun. 2005;73:1907–16.
31. Zheng W, Liu T, Sun R, et al. Daidzein induces choriocarcinoma cell apoptosis in a dose-dependent manner via the mitochondrial apoptotic pathway. Mol Med Rep. 2018;17:6093–9.
32. Lo YL. A potential daidzein derivative enhances cytotoxicity of epirubicin on human colon adenocarcinoma Caco-2 cells. Int J Mol Sci. 2012;14:158–76.
33. Huang N, Li P, Sun X, et al. TRIM21 mediates the synergistic effect of Olaparib and Sorafenib by degrading BRCA1 through ubiquitination in TNBC. NPJ breast cancer. 2023;9:85.
34. Liu YX, Wan S, Yang XQ, et al. TRIM21 is a druggable target for the treatment of metastatic colorectal cancer through ubiquitination and activation of MST2. Cell Chem Biol. 2023;30:709-725.e706.
35. Gao Z, Xu J, Fan Y, et al. ARPC1B promotes mesenchymal phenotype maintenance and radiotherapy resistance by blocking TRIM21-mediated degradation of IFI16 and HuR in glioma stem cells. J Exp Clin Cancer Res: CR. 2022;41:323.
36. Yuan J, Zhu Z, Zhang P, et al. SKP2 promotes the metastasis of pancreatic ductal adenocarcinoma by suppressing TRIM21-mediated PSPC1 degradation. Cancer Lett. 2024;587:216733.
37. Yang L, Zhang T, Zhang C, et al. Upregulated E3 ligase tripartite motif-containing protein 21 in psoriatic epidermis ubiquitylates nuclear factor-κB p65 subunit and promotes inflammation in keratinocytes. Br J Dermatol. 2021;184:111–22.
38. Koh M, Lim H, Jin H, et al. ANXA2 (annexin A2) is crucial to ATG7-mediated autophagy, leading to tumor aggressiveness in triple-negative breast cancer cells. Autophagy. 2024;20:659–74.
39. Ma S, Lu CC, Yang LY, et al. ANXA2 promotes esophageal cancer progression by activating MYC-HIF1A-VEGF axis. J Exp Clin Cancer Res: CR. 2018;37:183.
40. Gounou C, Rouyer L, Siegfried G, et al. Inhibition of the membrane repair protein annexin-A2 prevents tumor invasion and metastasis. Cell Mol Life Sci: CMLS. 2023;81:7.
41. Rocha MR, Barcellos-de-Souza P, Sousa-Squiavinato ACM, et al. Annexin A2 overexpression associates with colorectal cancer invasiveness and TGF-ß induced epithelial mesenchymal transition via Src/ANXA2/STAT3. Sci Rep. 2018;8:11285.
42. Tetsu O, McCormick F. Beta-catenin regulates expression of cyclin D1 in colon carcinoma cells. Nature. 1999;398:422–6.
43. Wang Q, Zhou Y, Rychahou P, et al. Deptor is a novel target of Wnt/β-catenin/c-Myc and contributes to colorectal cancer cell growth. Can Res. 2018;78:3163–75.
44. Wu J, Feng X, Du Y, et al. β-catenin/LIN28B promotes the proliferation of human choriocarcinoma cells via Let-7a repression. Acta Biochim Biophys Sin. 2019;51:455–62.
45. Tang T, Guo C, Xia T, et al. LncCCAT1 promotes breast cancer stem cell function through activating WNT/β-catenin signaling. Theranostics. 2019;9:7384–402.
46. Paunović MG, Matić MM, Obradović AD, et al. Antiproliferative, antimigratory, and prooxidative potential of novel platinum(IV) complexes and resveratrol on breast cancer (MDA-MB-231) and choriocarcinoma (JEG-3) cell lines. Drug Dev Res. 2022;83:688–98.
47. Gano CA, Fatima S, Failes TW, et al. Anti-cancer potential of synergistic phytochemical combinations is influenced by the genetic profile of prostate cancer cell lines. Front Nutr. 2023;10:1119274.

Publisher's Note